A Neutron Diffraction Study of the Electrochemical Double Layer Capacitor Electrolyte Tetrapropylammonium Bromide in Acetonitrile

Elizabeth K. Humphreys[1], *Phoebe K. Allan*[1,2], *Rebecca J. L. Welbourn*[3], *Tristan G. A. Youngs*[4], *Alan K. Soper*[4], *Clare P. Grey*[1], *Stuart M. Clarke**[3]

[1]Department of Chemistry, University of Cambridge, Lensfield Road, Cambridge, CB2 1EW

[2]Gonville and Caius College, Trinity Street, Cambridge, CB2 1TA

[3]BP Institute, University of Cambridge, Madingley Road, Cambridge, CB3 0EZ

[4]ISIS Facility, STFC Rutherford Appleton Laboratory, Harwell Oxford, Didcot, OX11 0QX

ABSTRACT

Neutron diffraction with isotopic substitution has been used to characterise the bulk liquid structure of the technologically relevant electrolyte solution, 1 M tetrapropylammonium bromide (TPA Br) in acetonitrile (acn), and of pure deuterated acetonitrile. Empirical potential structure refinement modelling procedures have been used to extract detailed structural information about solvent-solvent, solvent-ion and ion-ion correlations. Analysis of the refined data shows the expected local dipolar conformation of acn in the pure solvent. This short range dipolar ordering is also present within the solutions of TPA Br in acn, and it affects how the solvent orders itself around the ions. The solvation numbers of the TPA cations and the bromide anions are deduced – 8 and 5 respectively – as are the orientations of the solvent molecules surround the ions. Evidence for ion association is also presented, with nearly two thirds of the ions in the system being in associated pairs or clusters.

KEYWORDS: Neutrons; neutron diffraction; neutron scattering; electrochemical double layer capacitors; empirical potential structure refinement; EPSR; partial structure factors; partial pair distribution functions

INTRODUCTION

Electrolyte solutions are important in many different fields - from biologically important solutions, to technologically relevant ones. Their properties depend on both solvent and salt, as well as on how these interact. Low concentration (< 0.01 M) ionic solution behaviour is reasonably well understood in the bulk. It can be assumed that that there is little interaction between the salt ions and there are a number of theories describing how to calculate solution properties (such as conductivity, activity coefficients and diffusion).[1,2,3] However, as the concentration of ions increases, the interactions between all the different species can no longer be ignored and the solution behaviour becomes more complex.[1,3,4] Understanding high concentration electrolyte solution behaviour is key to understanding the many systems that utilise them.

One such technology that uses high concentration electrolyte solutions is electrochemical double layer capacitors (EDLCs). These high power energy storage devices use the physical mechanism of charge separation across the electrode/electrolyte interface to store energy.[5] As such, to further the understanding of the charge storage mechanism in EDLCs, we must clarify the behaviour of electrolyte solutions at the electrode interface, and the structures adopted by the ions and solvent molecules. However, in order to obtain molecular level insight into the electrode/electrolyte interface we must first understand the molecular level structure of the bulk electrolyte solutions. This is the focus of the present work.

There are a number of techniques available to study solution behaviour. Electrochemical techniques provide insight into the properties of electrolyte solutions,[2] however, if we are to identify the molecular level behaviour that gives rise to solution electrochemical processes, we need to utilise techniques that probe molecular level structure. Spectroscopic techniques, such as

Raman and Infrared, have previously been used to provide insight into how dissolved ions affect the structure of water and its hydrogen bonding network.[6,7] Changes in the O-H vibrational bands due to interactions with ions can also be used to extract information on ion solvation - such as coordination number and first solvation shell distance.[8,9,10] Studies of this type have also been performed on non-aqueous electrolytes.[11,12,13,14,15] Infrared, Raman and Nuclear Magnetic Resonance spectroscopies can also be used to study the conformations of more complex molecules in electrolyte solutions,[16,17,18,19,20] with the different techniques probing different timescales.

However, while these methods are able to provide helpful insights into the molecular level structure of parts of the solution, they generally cannot provide a fully comprehensive picture. In order to obtain a full molecular scale structural description, diffraction methods are typically used. While Bragg diffraction only provides information on long range order,[21] making it unsuitable for studying liquid structures, total-scattering methods also consider diffuse scattering. This provides information on non-periodic, disordered structures, making it an ideal tool for studying liquids.[22,23]

In the case of electrolyte solutions, neutron total-scattering is particularly suitable due to its ability to give accurate information about light elements, which is generally lacking in X-ray techniques.[24] Neutron diffraction is also isotope specific, allowing different contributions to the structural correlations to be separated out by measuring samples with different isotopic substitutions.[24]

Neutron scattering, in combination with empirical potential structure refinement modelling techniques, has previously been used to study the structures of a number of aqueous electrolyte solutions.[25,26,27,28] These studies give insight into each of the three main types of structural

correlation within electrolyte solutions: water-water, water-ion and ion-ion. In particular, Botti and co-workers[26] were able to distinguish between fully dissociated HCl and those H^+ and Cl^- ions that form ion pairs. Neutron scattering is not limited to simple aqueous electrolyte systems. Simple electrolytes based on other solvents have also been studied[29], as have more complicated systems involving ionic liquids, both in the case of the pure systems[30,31,32] and solutions where the ionic liquid has been used as a solvent[33,34]. In the present work, we use neutron total scattering to study different isotopic compositions of tetrapropylammonium bromide (TPA Br) in acetonitrile (acn), an electrolyte closely related to those used in commercial devices (e.g. tetraethylammonium tetrafluoroborate in acetonitrile). This solution was chosen not only as a close analogue to commercial electrolytes, but also for its structural properties. While acn is a widely used electrolyte solvent, it has the added benefit of a relatively simple structure. The bromide anion is monatomic, reducing the complexity of its related structural correlations and making distances associated with it relatively easy to assign. The TPA salt was chosen as although the cation is more complex than the other components of the solution, it gave the best balance between solution concentration and structural simplicity.

Previous studies on acn have shown that the partial charges in the molecule (a negative nitrogen end and a positive methyl end giving a dipole moment 3.93 D[35]) lead to local dipolar ordering in the form of anti-parallel pairs of molecules.[36,37,38,39,40,41] This dipolar ordering may lead to small clusters of anti-parallel pairs, but does not cause any extended long-range order within the liquid.[40,41] Investigations into TPA in solution have indicated that the alkyl chains adopt a trans configuration to minimise steric repulsion.[18,42] The effect of tetraalkylammonium cations on water molecules hydrating it in solution has also been studied. Enhanced hydrogen bonding of the water immediately surrounding TPA cation, and the similarly sized

tetrabutylammonium cation has been reported.[42,43] Pairing of the cation with its anion has also been seen, as has slight penetration of the anion into the cation structure.[44,20] In addition to cation-anion association, contact between the alkyl chains of tetraalkylammonium cations in high concentrations has also been noted.[45,20] Studies on bromide anions have mostly considered its solvation. Generally the solvation by the methyl group of acn molecules is within around 4 Å.[46,47,48] There is more variation in the reported solvation number of bromide by acn, which ranges from 4 to 10.[46,48]

In this paper we analyse the structures of pure acn and TPA Br in acn solution using neutron scattering combined with empirical potential structure refinement (EPSR) analysis. EPSR analysis was used to allow an in depth investigation into the structure of the liquids studied (more detail on EPSR and the information it allows access to is given in the Empirical Potential Structure Refinement section below). Partial pair distributions calculated using EPSR are used to investigate the dipolar ordering and coordination number of the pure acn. They are also used to examine the changes in acn between the pure solvent and the TPA Br in acn solution; as well as the solvation of the ions in solution and the ion-ion interactions.

NEUTRON SCATTERING THEORY

As details of both neutron scattering theory and the technique of isotopic substitution have been described before,[49,50] only a brief outline of the theory will be provided here.

In a neutron scattering experiment, the total scattered intensity of a sample is measured as a function of the momentum transfer vector ($Q = \frac{4\pi \sin\theta}{\lambda}$, where 2θ is the scattering angle and λ is the wavelength of the incident neutron). This measured intensity is then corrected for

experimental factors (such as background scattering, absorption and inelastic scattering) to give the total structure factor:

$$F(Q) = \sum_{\alpha\beta} c_\alpha c_\beta b_\alpha b_\beta \left[S_{\alpha\beta}(Q) - 1\right]$$

where c are the atomic concentrations, b are the coherent neutron scattering lengths, and $S_{\alpha\beta}(Q)$ are the partial structure factors for all the atoms present in the sample.[49,50]

The partial structure factors, $S_{\alpha\beta}(Q)$, and the total structure factor, $F(Q)$, are related to the partial and total pair distribution functions, $g_{\alpha\beta}(r)$ and $G(r)$ respectively, by the Fourier transformations:[22,51]

$$g_{\alpha\beta}(r) = \frac{2}{\pi}\int_0^\infty Q\left[S_{\alpha\beta}(Q) - 1\right]\sin(Qr)\,dr$$

$$G(r) = \frac{2}{\pi}\int_0^\infty Q[F(Q) - 1]\sin(Qr)\,dr$$

These pair distribution functions (PDFs) are real space correlation functions that provide a weighted histogram of the atom-atom distances within a material. The total PDF provides information on all of the atom pairs within a material. The partial PDFs (pPDFs) give only the distances between two types of atom within a material, α and β (for example in a solution of lithium bromide in water, one pPDF would describe the distances between the lithium cations and the oxygen atoms on the water). The peaks in total PDF are weighted by the scattering lengths of the atoms involved.

Another real space correlation function that can be calculated from diffraction data is the total pair correlation function, $f(r)$. While very similar to the total PDF, it is normalised in a different manner, giving a somewhat different appearance to the two functions. $G(r)$ tends to 0 at $r = 0$ with a slope of $-4\pi\rho$, and oscillates around 0 at high-r. $f(r)$ also oscillates around 0 at high-r,

however, at low-r it goes to the negative of the neutron weighting of the sample ($-\langle cb\rangle^2$, where c and b are the atomic fraction and coherent scattering of the different components of the system).[51]

The total pair correlation function, $f(r)$, is related to the total PDF by the following equation:

$$G(r) = 4\pi\rho r f(r)$$

where ρ is the density of the sample and r is the inter-atomic spacing between atom pairs. Both $G(r)$ and $f(r)$ can be used when considering the real space correlations found within a sample.

As described above, neutron scattering lengths are both isotope specific and vary in a non-systematic way across the periodic table. These properties stem from the fact that neutrons interact with matter via the nuclei of the sample atoms, rather than via electrons as is the case for X-rays. The technique of neutron scattering with isotopic substitution takes advantage of the isotope specificity of neutron scattering to gain extra structural information.

If multiple samples are chemically the same, except for isotope exchange of one type of atom, then their structures can be assumed to be essentially identical. However, as the total structure factor is dependent on the scattering power of the atoms involved, the samples will provide different neutron scattering patterns. The difference between the scattering of the isotopically substituted samples can then be used to extract a partial structure factors, and hence pPDFs. A full mathematical description of how these partial structure factors are calculated can be found in the paper by Bowron *et al*[50].

How isotopic substitution affects scattering patterns can be illustrated by considering a solute (A), which can be isotopically substituted, dissolved in a solvent. Using two samples, where each is fully composed of one isotope of A (A_1 or A_2), a first order difference can be performed.

Subtracting one scattering pattern from the other will cause all the components related to the solvent to cancel. This will leave the scattering components between A and the solvent, and between the molecules of A. To extract purely the scattering between the molecules of the solute, a second order difference experiment is required. This involves three samples: one sample for isotope A_1, one sample for isotope A_2 and one containing a mixture of A_1 and A_2. This is illustrated in Figure 1 and Figure 2. The full mathematical description of first and second order difference experiments is also found in Bowron *et at*[50].

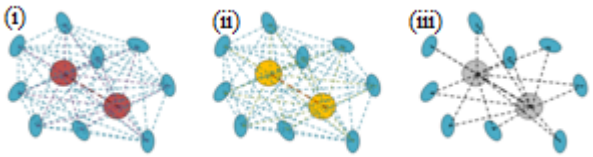

Figure 1: Schematic of the interactions in solution samples and those seen after first order difference analysis. Blue ellipses represent solvent molecules (S), circles represent the solute, A (red for isotope A_1, yellow for isotope A_2, and grey for difference data), and dashed lines represent the interactions seen in each sample. i) A_1 solution sample, interactions: S--S, A_1--S, A_1--A_1; ii) A_2 solution sample, interactions: S--S, A_2--S, A_2--A_2; iii) First order difference (A_1 - A_2), interactions: [A_1--S - A_2--S], [A_1--A_1 - A_2--A_2]

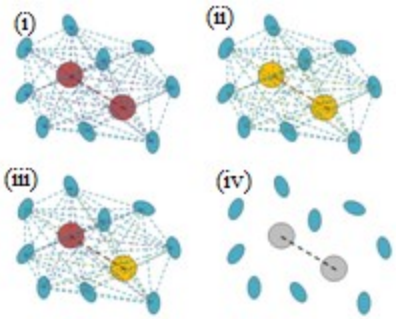

Figure 2: Schematic of the interactions in solution samples and those seen after second order difference analysis. Symbols have the same meaning as in Figure 1. i) A_1 solution sample, interactions: S--S, A_1--S, A_1--A_1; ii) A_2 solution sample, interactions: S--S, A_2--S, A_2--A_2; iii) A_1A_2 solution sample, interactions: S--S, A--S (0.5*A_1--S + 0.5*A_2--S), A--A (0.25*A_1--A_1+ 0.25*A_2--A_2 + 0.5*A_1--A_2); iv) Second order difference (A_1 + A_2 - 2*A_1A_2), interactions: A_1--A_2

EMPIRICAL POTENTIAL STRUCTURE REFINEMENT

Interpretation of the PDFs generated from experimental neutron scattering data can be done in a number of ways. In some cases the peaks within these real space functions can be directly related to a simple structural model. For liquids, this can only be done conveniently for the peaks corresponding to the short, intramolecular distances. At higher-r, where the distances correspond to those between molecules, the peaks broaden due to the number of atom-atom separations contributing similar values. This makes direct analysis more challenging.

As such, for liquids it is common to utilise some form of modelling against the data generated during the experiment. One such method is Empirical Potential Structure Refinement (EPSR).[52] EPSR utilises a Monte Carlo style approach to minimise the difference between experimental diffraction data and diffraction patterns generated from the simulation of the structure.[52,53,54]

Initial structures for an EPSR simulation are generated by placing the appropriate number of molecules into a box to give the required density. The potential of the simulation box is calculated using the following equation:

$$U_{tot} = U_{intra} + \sum_{\alpha\beta}\left(4\varepsilon_{\alpha\beta}\left[\left(\frac{\sigma_{\alpha\beta}}{r_{ij}}\right)^{12} - \left(\frac{\sigma_{\alpha\beta}}{r_{ij}}\right)^{6}\right] + \frac{q_\alpha q_\beta}{4\pi\varepsilon_0 r_{ij}}\right) + U_{EP}$$

where U_{intra} is described using a series of harmonic potentials, $\varepsilon_{\alpha\beta}$ and $\sigma_{\alpha\beta}$ are the Lennard-Jones parameters for the potential well depth and effective atom size, r_{ij} is the inter-atomic spacing, q_α are the atomic charges and ε_0 is the vacuum permittivity. U_{EP} is the empirical potential, which is calculated from the difference between the experimental scattering pattern and the scattering pattern generated by the simulated structure.[53,54]

In conventional Monte Carlo simulation, atomic and molecular moves are accepted or rejected on the basis of the change in configurational energy which results from the move. If the configurational energy falls the move is always accepted, whereas if the energy increases, the move is only accepted on the basis of a Boltzmann probability distribution. Hence large increases in energy will be accepted only rarely. In EPSR exactly the same principle applies. The difference with conventional MC is simply that the potential energy function has an additional, perturbative term derived purely from the fit of the simulation to the scattering data. This empirical potential energy term serves to drive the simulated structure as close as possible to the scattering data, without violating the constraints imposed on atomic overlap, van der Waals forces, and hydrogen-bonding which are present in all computer simulations of fluids. [53,54]

A large range of information is available from the final EPSR simulated structures - from pPDFs to specific inter-atomic distances and distributions of intramolecular atom separations.

This allows for more detailed analysis of complicated or disordered structures than would be available just by examining the experimental data directly.

EXPERIMENTAL METHODS

Neutron diffraction data were collected on seven different isotopic compositions of 1 M TPA Br in acn (Table 1). These compositions were chosen to allow second order difference calculations to be performed for both the cation and the solvent hydrogen atoms. Data were also recorded for the pure solvent, deuterated-acn, in order to help with the assignment of structural correlations in the electrolyte solution. The number of contrasts measured for the pure acn was ultimately limited by the amount of allocated beamtime. The weightings of a selection of the pPDFs for each sample is given in Table 2 (for the full list of weightings see supplementary information Tables S14 and S19)

Table 1: Solution isotopic compositions

TPA Br	**acn**
h[a]	h
d[b]	h
h	d
d	d
1:1 h/d[c]	d
d	1:1 h/d[d]
1:1 h/d	1:1 h/d

a - h, hydrogenated; b - d, deuterated; c - 1:1 mixtures measured by mass; d - 1:1 mixture measured by volume

Table 2: weightings of the pPDFs in the different samples, calculated from $c_\alpha c_\beta b_\alpha b_\beta$ where c_i and b_i are the atomic fraction and coherent scattering length of species i.

Sample	C_1--C_1	C_1--N_1	N_1--N_1	N_{1c}--C_1	N_{1c}--N_1	Br_1--C_1	Br_1--N_1
d-acn	1.2247	1.2247	3.6907	--	--	--	--
h in h	0.6577	0.6577	-1.1114	0.0483	0.0681	0.0351	0.0495
h in d	0.6577	0.6577	0.0000	0.0483	0.0681	0.0351	0.0495
d in h	0.6577	0.6577	-1.1114	0.0483	0.0681	0.0351	0.0495
d in d	0.6577	0.6577	0.0000	0.0483	0.0681	0.0351	0.0495
1:1 in d	0.6577	0.6577	0.0000	0.0483	0.0681	0.0351	0.0495
d in 1:1	0.6585	0.6585	-0.5554	0.0483	0.0682	0.0351	0.0495
1:1 in 1:1	0.6585	0.6585	-0.5554	0.0483	0.0682	0.0351	0.0495

Sample	N_{1c}--N_{1c}	N_{1c}--Br_1	Br_1--Br_1
d-acn	--	--	--
h in h	0.0035	0.0101	-0.0397
h in d	0.0035	0.0101	-0.0397
d in h	0.0035	0.0101	0.0000
d in d	0.0035	0.0101	0.0000
1:1 in d	0.0035	0.0101	-0.0198
d in 1:1	0.0035	0.0101	0.0000
1:1 in 1:1	0.0035	0.0101	-0.0199

The hydrogenated and deuterated acetonitrile were obtained from Sigma Aldrich (ACS reagent, ≥99.5%) and VWR International (purity 99.9%, isotopic enrichment ≥99.8%) respectively; while the hydrogenated and deuterated tetrapropylammonium bromide salts were

obtained from Alfa Aesar (purity ≥98%) and CDN Isotopes (purity ≥99%, isotopic enrichment ≥98%) respectively. All materials were used as received.

Scattering experiments were carried out at the Near and Intermediate Range Order Diffractometer beamline[55] (NIMROD) of Target Station Two at the ISIS neutron spallation source at the Rutherford Appleton Laboratory. NIMROD has an available neutron wavelength range from 0.05 to 14 Å. It uses ZnS scintillator detectors, which are placed forward of the sample position and collect data up to scattering angles ~45°. This arrangement serves to minimise neutron inelasticity effects from materials which contain hydrogen. Samples were contained in TiZr alloy cells with internal dimensions of 35 mm by 35 mm by 1 mm. PTFE o-rings were used to provide an air-tight seal to the cells and prevent solvent evaporation during the experiments, since data were collected under vacuum.

Data were collected up to 50 $Å^{-1}$ with a count time of 210 minutes and a beam size of 30 mm by 30 mm. A 35 mm by 35 mm by 3 mm vanadium plate and the straight-through beam (no sample between the incident beam and the detector) were each measured for 60 minutes for normalisation corrections. Empty TiZr alloy sample cells were also measured for 60 minutes for background corrections.

Data were merged from all detectors, and standard corrections for detector 'dead-time', multiple scattering, attenuation and single-atom scattering were applied to the raw data using Gudrun software[56]. Gudrun was also used to carry out corrections for inelasticity effects. These corrections were carried out in the manner detailed by Soper[57].

Once corrected, data were normalised and Fourier transformed in the Q range of 0.01 to 50 A^{-1} to generate pair correlation functions, $f(r)$, and pair distribution functions, $G(r)$, using this

program. The density of the d-acn was taken to be 0.844 g cm^{-3},[58] while the densities of the solutions were calculated based on the mass of each sample and the volume of the TiZr cells.

EPSR simulations were set up using a cubic box containing 1008 molecules. For the acn simulation this gave a box side length 44.38 Å, while for the solution simulation this gave a box side length of 46.96 Å. It also leads to a distribution of molecules in the solution simulation box of 912 acn molecules, 48 TPA cations and 48 Br anions. The parameters used to describe the molecules in the simulations are detailed in the supplementary information (Section S1). Before setting up the simulation boxes, energy minimisation was run on the template molecules using MOPAC[59] with the AM1 Hamiltonian. The minimised templates were combined to give the simulation boxes, which were then run with EPSR to minimise the box energy. Details of the simulations can be found in the supplementary information (Section S2).

RESULTS AND DISCUSSION

DEUTERATED ACETONITRILE

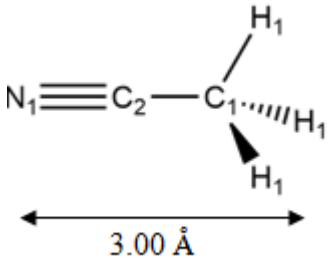

Figure 3: The structure of d-acn with labels used in EPSR analysis. The scale indicates the distance between the centre of the nitrogen atom and the centre of a hydrogen atom projected in line with the main bond axis.

Figure 3 shows a schematic of an acetonitrile molecule, with the labels used in the subsequent analysis.

Figure 4 shows the experimental structure factor, $F(Q)$, for d-acn and the function generated by the EPSR simulation. There is good agreement between the experimental data and the EPSR fit down to approximately 1 Å^{-1}. The difference between the two functions at these low Q values is due to the finite size of the simulation box (this is illustrated in the supplementary information, Section S3, Figure S3).

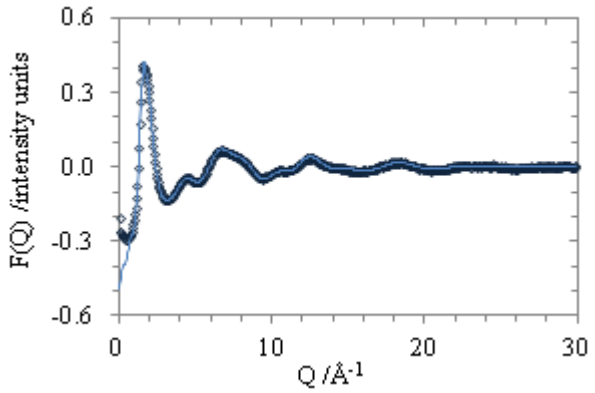

Figure 4: Experimentally determined (points) and EPSR simulated (solid line) $F(Q)$ for d-acn.

Figure 5a, b and c show the d-acn pair correlation functions, $f(r)$, calculated from the experimental Q data and the simulation, for the distances ranges 0-20 Å, 0-5 Å and 3-18 Å respectively. Peaks below 3.2 Å have been assigned to intramolecular distances (see Table 3). The peak positions are consistent with values in the literature (determined using electron, neutron and X-ray diffraction),[60,61,62,63,64,36] giving confidence in the quality of the experimental data and the approach used to interpret it.

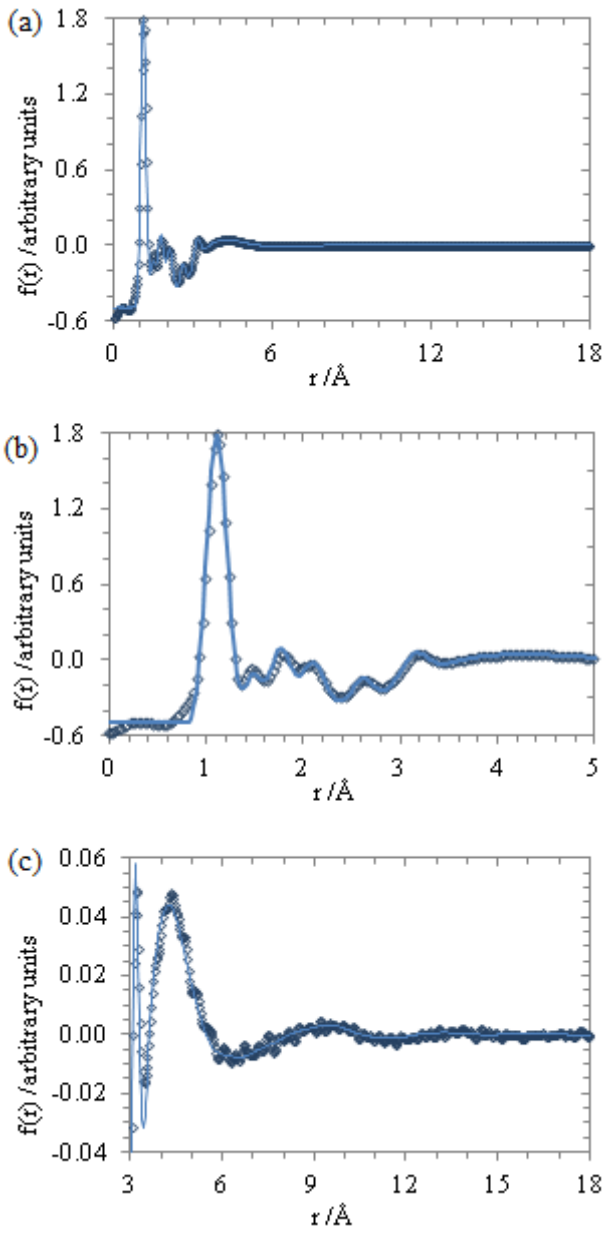

Figure 5: $f(r)$ calculated from the experimental Q data (points) and the EPSR simulation (solid line) for d-acn for a) 0-20 Å; b) 0-5 Å; c) 3-18 Å.

Table 3: Assignment of low-r peaks for d-acn $f(r)$ and comparison with literature data

peak position[a] /Å	**assignment**	**literature values /Å**
1.11	N_1-C_2 (triple bond)	N_1-C_2: 1.16[b], 1.16[c], 1.16[d], 1.15[e], 1.17[f], 1.14[g]

	C_1-H_1 (single bond)	C_1-H_1: 1.10[d], 1.08[f]
1.46	C_1-C_2	1.49[b], 1.47[c], 1.46[d], 1.47[e], 1.46[f], 1.48[g]
1.77	H_1-H_1	
2.11	C_2-H_1	2.09[e], 2.09[f], 2.12[g]
2.60	N_1-C_1	
3.18	N_1-H_1	

a - peak positions taken directly from $f(r)$ plots by considering positions of peak maxima;
b-from ref [60]; c-from ref [61]; d-from ref [62]; e-from ref [63]; f-from ref [64]; g-from ref [36]

There is a clear broad peak between 3.5 Å and 5.5 Å in the high-r region (Figure 5c) from the intermolecular first nearest neighbour distances. A second, shallow peak is seen between 8.2 Å to 10.5 Å, from intermolecular second nearest neighbour distances; and a further very shallow peak is observed around 13.5 Å, which has been assigned to third nearest neighbour distances. The inherently disordered nature of liquid systems means that beyond this distance the structure is almost truly random, hence no further significant density fluctuations are seen. The high frequency noise in the $f(r)$ calculated from the experimental Q data comes from truncation errors during the Fourier transformation.

As with $F(Q)$, the pair correlation function calculated from the EPSR simulation provides a good fit to that calculated from the experimental data. The bond lengths, angles and atomic partial charges for the model were chosen based on the work by Nikitin and Lyubartsev.[65] Although there are slight discrepancies between the fit and the data for the position and area of the intramolecular peak around 1.76 Å and the area of the intramolecular peak around 1.46 Å, the agreement is generally good.

By considering the intermolecular pPDFs calculated using EPSR from the experimental data and the simulation we are able to investigate the positional and orientational ordering of the acn

molecules. The intermolecular C_1--C_1, C_1--N_1 and N_1--N_1 pPDFs are shown in Figure 6. The other pPDFs can be found in the supplementary information (Section S3, Figure S4).

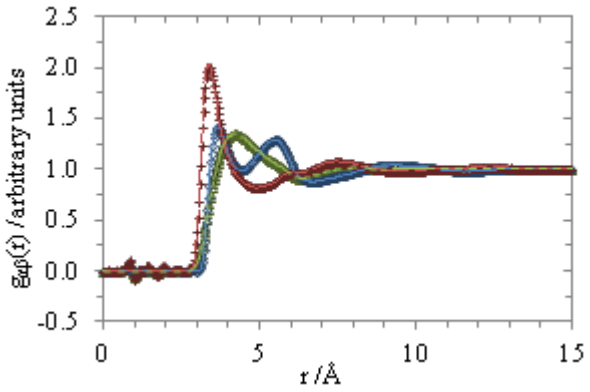

Figure 6: Intermolecular pPDFs calculated from the d-acn experimental data (points) and simulation (lines), for C_1--C_1 (blue diamonds and solid line), C_1--N_1 (red crosses and long-dashed line) and N_1--N_1 (green triangles and short-dashed line) atom pairs.

Acn is a dipolar molecule: the nitrogen end has a partial negative charge and the methyl end has a partial positive charge. In our simulations a dipole moment of 3.95 D is assumed based on our chosen partial charges. Therefore we would expect molecules to approach each other more closely with their oppositely charged ends, to maximise the dipolar interactions. This is reflected in the pPDFs in Figure 6 where the shortest and most clearly defined first peak is for C_1--N_1 at 3.4 Å (C_1--C_1 and N_1--N_1 first peaks occur at 3.8 Å and 4.1 Å respectively).

The coordination number of a molecule or an atom is determined by the number of other molecules or atoms that surround it. The coordination number of a given atom type within acn can be calculated by integrating the pPDFs between the appropriate values of r. Where there is a pronounced minimum in the pPDFs this is a reasonably well-defined quantity. However, in some cases there may be some uncertainty over which values are appropriate. Table 4 shows the C_1 and N_1 coordination over four distance ranges. These distance ranges have been chosen based on

positions of the minima after the peaks in the pPDFs. The C_1--N_1 coordination in the distances ranges 3.0 - 4.0 Å and 3.0 - 4.5 Å (2.7 and 3.9 respectively) is significantly higher than either the C_1--C_1 or N_1--N_1 coordination. As with the pPDFs showing that C_1--N_1 has the closest approach distance, this is related to maximising the favourable interactions between the dipoles of the acn molecules. Aligning the molecules such that their oppositely charged ends are closer than their like charged ends will maximise the favourable electrostatic interactions and so give the most energetically favourable configuration for the bulk fluid.

Table 4: C_1 and N_1 coordination numbers calculated by EPSR from d-acn pPDFs

partial	**distance range for N(r) /** Å			
	3.0 - 4.0[a]	**3.0 - 4.5[b]**	**3.0 - 5.0[c]**	**3.0 - 6.3[d]**
C_1--C_1	1.8 ± 1.0	3.0 ± 1.1	4.7 ± 1.2	11.8 ± 1.5
C_1--N_1	2.7 ± 1.0	3.9 ± 1.1	5.3 ± 1.2	10.8 ± 1.5
N_1--N_1	1.5 ± 1.0	3.3 ± 1.3	5.3 ± 1.4	11.3 ± 1.5

a - range to where C_1--N_1 first peak crosses C_1--C_1 first peak; b - range to first minima in C_1--C_1 pPDF; c - range to first minima in C_1--N_1 pPDF; d - range to first minima in N_1--N_1 pPDF

The average 3D spatial distribution of molecules around a central molecule is expected to show three-fold symmetry, to match that of the molecule itself. The spatial and orientational density functions of acn molecules surrounding a central acn molecule are shown in Figure 7a and 7b-c respectively. The spatial density function represents a three-dimensional map of the density of acn centre of mass positions relative to the central molecule, indicating the most likely relative positions of the acn molecules. The function shows the expected three-fold symmetry, indicating that steric considerations, as well as dipolar ordering, play a role in the local structure of the acn molecules. The orientational density functions represent the density of the centre of mass positions of acn molecules that obey certain orientational constraints. In this case, the

function shown in purple represents the positions of acn molecules that are parallel to the central molecule, while the yellow function represents the positions of acn molecules that are anti-parallel to the central acn molecule. The surrounding parallel molecules are positioned at either end of the central acn molecule. This will allow the most favourable interactions between the opposite ends of the dipole moment. At the methyl end of the central acn the surrounding parallel acn molecules are mostly found near the hydrogens, rather than in between. This will maximise the electrostatic interactions between the partial charges on the acn molecules, as although the methyl end has an overall positive charge, this comes from the charges on the hydrogen atoms as the C_1 methyl carbon carries a negative partial charge (for the full partial charge values see supplementary information Section S1.1 Table S2). The surrounding anti-parallel molecules are found mostly around the middle of the central molecule. This will allow both ends of each molecule to interact favourably, minimising any electrostatic repulsions between the partial charges. There is also a small area of anti-parallel molecules at the methyl end of the central acn molecule. This probably relates to two factors; the first is the density of parallel molecules in this region. As well as being anti-parallel to the central molecules, the anti-parallel molecules in this region are anti-parallel to the parallel molecules near the central acn hydrogens. This allows favourable interactions between the molecules surrounding the central acn. The second reason is that while the nitrogen end has a relatively large negative partial charge, the negative charge on the C_1 methyl carbon means that the positive charge of the methyl end has a smaller magnitude. This will decrease any unfavourable electrostatic interactions that occur between the two methyl ends of the acn molecules.

(a)

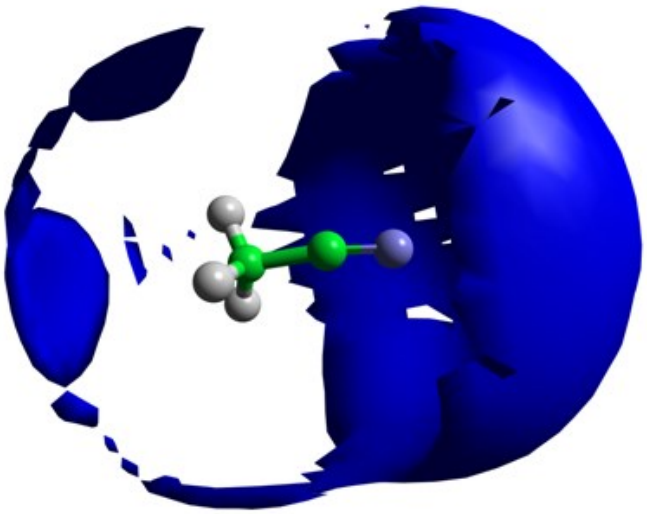

(b)

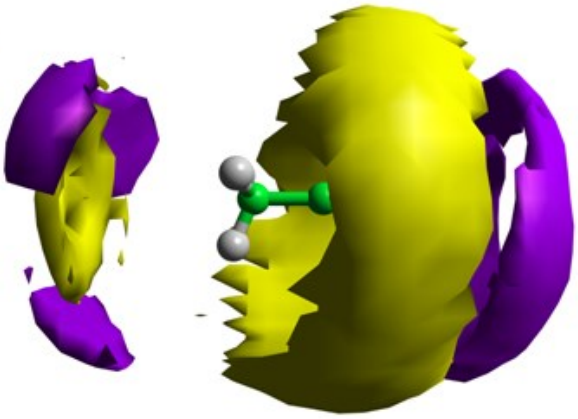

(c)

Figure 7: (a) Spatial density distribution function of acn molecules about a central acn molecule, encompassing a surface representing 2.5 times the bulk density of molecules in the system; (b-c) orientation density distribution function of acn molecules about a central acn molecules, where the surface represents high probability positions of molecules being aligned parallel (purple) or anti-parallel (yellow) within ± 10 °.

1 M TPA Br IN ACN SOLUTIONS

A schematic of a TPA cation is shown in Figure 8, including the labels used in the subsequent analysis. Each alkyl chain of the cation is labelled in the same manner (i.e. all four of the methyl carbon atoms are labelled C_{3c}). All of the hydrogen atoms within the cation are given the same label - H_{1c} - as the different hydrogen environments are not considered separately for the analysis.

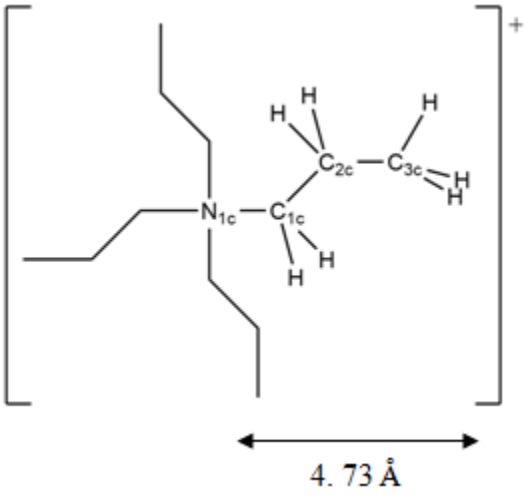

Figure 8: TPA cation showing nitrogen and carbon labels used in the subsequent analysis. For clarity, only one alkyl chain is labelled and the H atom labels are not shown. The scale indicates

the radial distance from the centre of the nitrogen atom to the centre of one of the methyl hydrogens.

The EPSR model for the 1 M TPA Br solution refined the simulation against all seven of the solution data sets simultaneously. This allowed the greatest accuracy with respect to the data to be achieved.

In Figure 9 the experimental $F(Q)$ for three of the seven solutions are shown, along with the simulated $F(Q)$ generated using EPSR (a larger version of this figure may be found in the supplementary information, section S4, Figure S5a). The structure factors for the other four solution compositions are shown in the supplementary information (Section S4, Figure S5b). As with the pure d-acn, there is good agreement between the experimental data and the EPSR model. Below 1 $Å^{-1}$ there is some divergence between the model and the experimental data; this is attributed to the finite size of the simulation box or to small contributions from residual inelasticity effects that have not been completely removed in the data analysis.

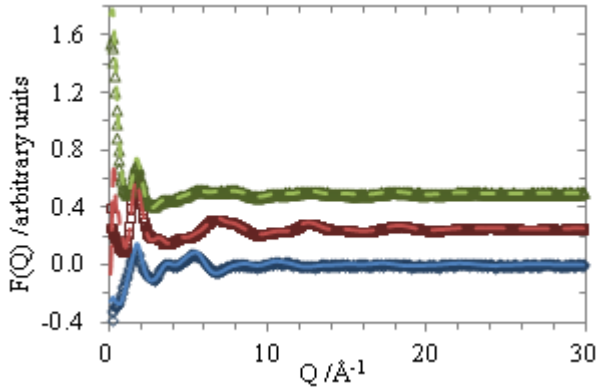

Figure 9: Experimentally determined (points) and EPSR simulated (lines) $F(Q)$ for h-TPA Br in h-acn (bottom, blue diamonds and solid line); d-TPA Br in d-acn (middle, red crosses and long dashed line); and 1:1 h/d-TPA Br in 1:1 h/d-acn (top, green triangles and short dashed line)

Figure 10a, b and c show the pair correlation functions, $f(r)$, calculated from the experimental d-TPA Br in d-acn Q data and from the EPSR simulation over different distance ranges (0-20 Å, 0-5 Å and 3-18 Å). This isotopic composition was chosen to illustrate the solution results as it is most readily comparable to the pure d-acn data and it only contains atoms with positive scattering lengths, making it visually the most simple. The pair correlation functions calculated for the other six isotopic compositions are shown in the supplementary information (section S4, Figure S6).

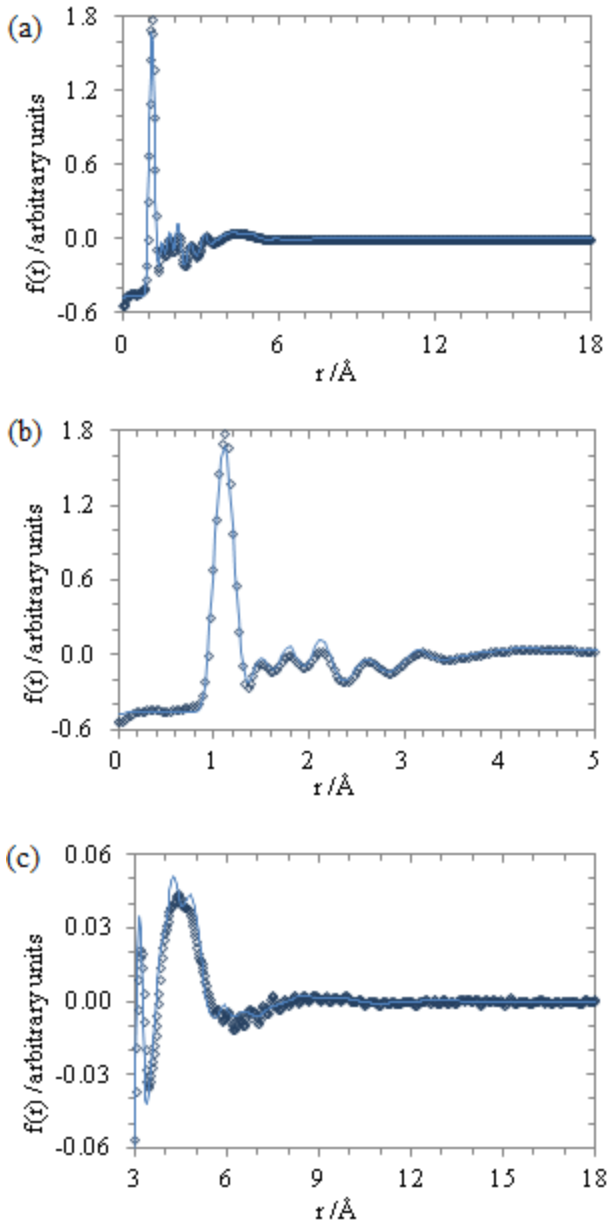

Figure 10: $f(r)$ calculated from experimental Q data (points) and EPSR simulation (lines) for d-TPA Br in d-acn solution for a) 0-20 Å; b 0-5 Å; c) 3-18 Å.

The TPA Br in acn solution $f(r)$ is very similar to that of pure d-acn. While the peaks at low-r have slightly different relative intensities between the solution and the pure solvent, the peak positions are virtually identical. The broader peaks at higher-r also cover similar distances ranges

in solution to the peaks in the pure solvent. There are two reasons for this similarity. Firstly, a 1M TPA Br in acn solution corresponds to a ratio of 19:1 acn to TPA Br, meaning that the pair correlation function is dominated by inter-solvent interactions. Secondly, acn and the TPA cation are expected to contain very similar intramolecular distances. Both molecules contain C-H single bonds and C-C single bonds, whose values are nearly identical between the two molecules (see supplementary information Tables S3 and S7 for initial template molecule bond lengths and Tables S12, S15 and S16 for the final simulation bond length distributions). The remaining bonds are also similar lengths to these; the N-C single bonds in the TPA cation having similar values to the C-C single bonds and the N-C triple bond on the acn having a similar value to the C-H single bonds. As such, the differences in $f(r)$ at low-r will be subtle.

The broader, intermolecular peaks at high-r (shown in Figure 10c) are less similar than the low-r peaks (in Figure 10b). The first broad peak, centred around 4.6 Å is related both to the first solvation shells of the ions and the first intermolecular distances of the acn molecules, as these are expected to be at similar distances. The second, shallower broad peak is observed between 8 Å and 10.4 Å. As with the pure acn, this is attributed to second intermolecular nearest-neighbour distances (including second solvation shell distances for the ions). This peak begins at a slightly shorter distance in solution than the corresponding peak in the pure acn $f(r)$. This is presumably related to the presence of the ions, as they will hold their solvation shells more closely than the acn molecules will hold their coordination shells due to the electrostatic interactions with the partial charges on the acn molecules. Unlike the d-acn, there is no third very shallow peak in the solution $f(r)$. The lack of any significant structure beyond 11 Å is, as with the pure acn, due to the disordered nature of liquid systems. Also, the high frequency truncation error ripples observed in the acn $f(r)$ are seen for the solution data.

The agreement between the $f(r)$ calculated from the EPSR simulation and that obtained from the experimental data is similar to that seen for the d-acn. The main difference between the $f(r)$ calculated from the data and from the simulation is observed in the intermolecular first nearest neighbour peak centred around 4.5 Å. The simulated pair correlation function shows a substructure (two sub-peaks at 4.3 Å and 4.8 Å are observed) that is not immediately apparent within the pair correlation function calculated from the experimental data.

It is likely that this sub-structure is mostly due to an overly ordered configuration of the TPA cation. However, as the main focus of the present work is on the intermolecular interactions, the extra order is relatively insignificant when the pair correlation function is considered as a whole.

Analysis of the pPDFs calculated by EPSR from the experimental data and simulations allows us to compare any acn ordering to that in the pure solvent, and to examine the solvation structures of the ions and any ion-ion correlations. The full set of pPDFs is shown in the supplementary information (Section S4, Figures S7 to S12).

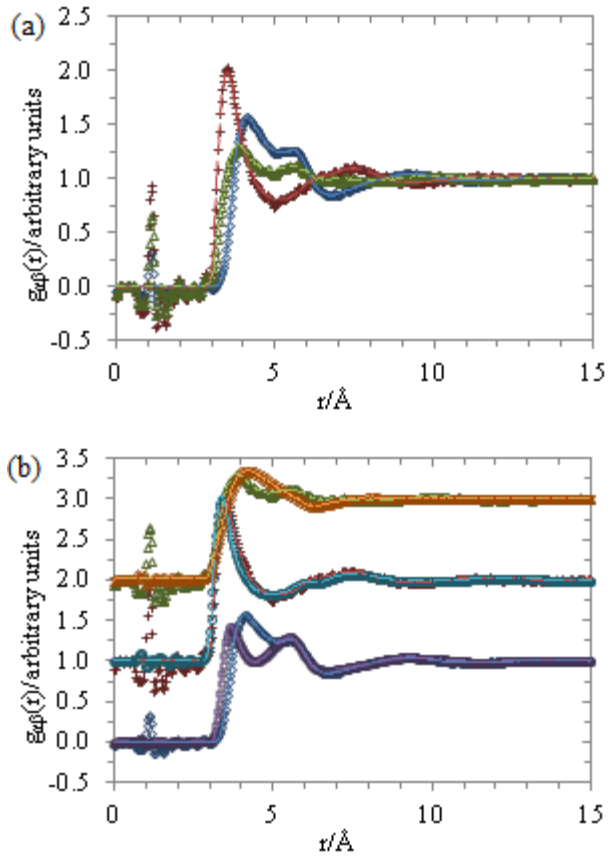

Figure 11: (a) Intermolecular pPDFs calculated from experimental data (points) and simulation (lines) for C_1--C_1 (blue diamonds and solid line), C_1--N_1 (red crosses and long-dashed line) and N_1--N_1 (green triangles and short-dashed line) for the solution; (b) Comparison of the C_1--C_1, C_1--N_1 and N_1--N_1 pPDFs for the solution (points and lines as in (a)) and the pure solvent (C_1--C_1 purple squares with dash-dot-dot line, C_1--N_1 pale blue circles with dash-dot line and N_1--N_1 orange x's with dotted line)

It can be seen in Figure 11a that, as with the pure acn solvent, the C_1--N_1 pPDF shows the closest approach (peak at 3.5 Å) of the three key acn intermolecular distances. The C_1--N_1 first peak also continues to be the sharpest of the three. This indicates that the dipolar ordering is still present within the solution. However, this peak is at a slightly higher-r value than in the pure d-

acn, as seen in Figure 11b. This figure also shows that the first peaks in the C_1--C_1 and N_1--N_1 pPDFs have also moved - the C_1--C_1 peak position increasing from 3.8 Å in the pure solvent to 4.1 Å in the solution and the N_1--N_1 peak position decreasing from 4.1 Å to 3.8 Å. The near edge of the first peak in the N_1--N_1 pPDF is also slightly steeper than in the pure solvent. These changes are attributed primarily to the altered ordering of the acn molecules in the first solvation shells of the ions due to the electrostatic interactions between the ions and the acn partial charges. These interactions are likely to orient the acn molecules with parallel dipoles, disrupting the previous anti-parallel ordering near the ions. This is in contrast to the effect of tetraalkylammonium ions in water, where they enhance the hydrogen bonding network.[42,43]

The coordination of the C_1 and N_1 atoms in solution calculated using EPSR for four distance ranges are given in Table 5. The same distance ranges as the pure d-acn have been used to allow the best comparison. It can be seen that for each distance range, there is a slight decrease in the coordination number relative to the pure solvent. This may indicate that the acn molecules in the solvation shells of the ions are slightly less densely packed than in the bulk. The errors in the coordination numbers are slightly larger in the solution compared to the pure d-acn. This is probably due to the reduced number of acn molecules in the solution simulation used to give the same total number of units.

Table 5: C_1 and N_1 coordination numbers calculated from solution pPDFs

partial	**distance range for N(r) / Å**			
	3.0-4.0	**3.0-4.5**	**3.0-5.0**	**3.0-6.3**
C_1--C_1	1.0 ± 0.9	2.5 ± 1.2	4.2 ± 1.4	9.4 ± 1.9
C_1--N_1	2.1 ± 1.1	3.1 ± 1.2	4.2 ± 1.4	8.3 ± 1.8
N_1--N_1	1.3 ± 1.0	2.4 ± 1.2	3.8 ± 1.4	8.8 ± 1.9

Insights into the solvation of the TPA and Br ions can be derived from the pPDFs for the ion-acn intermolecular interactions, shown in Figure 12.

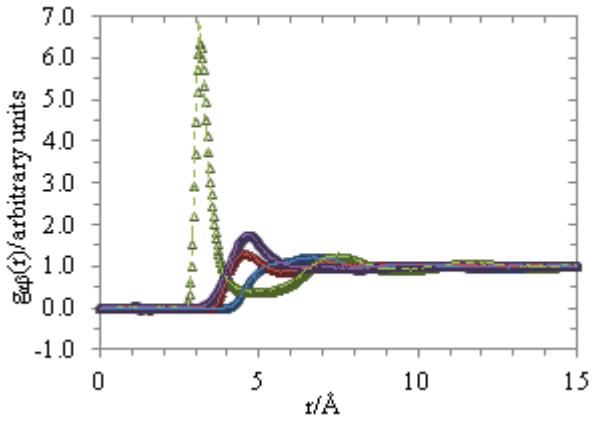

Figure 12: Intermolecular pPDFs calculated from experimental data (points) and simulation (lines) for C_1--N_{1c} (blue diamonds, solid line), N_1--N_{1c} (red crosses, long-dashed line), C_1--Br_1 (green triangles, short-dashed line) and N_1--Br_1 (purple squares, dash-dot-dot line)

The first peak in the N_1--N_{1c} pPDF is both sharper and at a shorter distance than the first peak in the C_1--N_{1c} pPDF (4.5 Å and around 6.2 Å respectively), due to the favourable interaction with the slightly negative nitrogen end of the acn. The separation between the centres of these peaks is a little under 2 Å. This indicates that the acn molecules do not come out directly radially from the TPA cations, but at an angle. By comparing the ion-acn distances with the intramolecular acn distances, and angle of 63 ° has been calculated (for details of the calculation see the supplementary information section S4). The radius of the TPA cation is estimated to be a little over 5 Å (from the bond lengths used to create the TPA model and the van der Waals radius of hydrogen). As the first peak in the N_1--N_{1c} pPDF is below this value it may indicate that there is some solvent penetration between the alkyl chains towards the centre of the cation. Such

penetration would presumably not go particularly far into the volume of the cation as the methylene groups are likely to be quite closely packed.

The peaks in the C_1--Br_1 and the N_1--Br_1 pPDFs are sharper than those in the partials involving the cation, particularly the first peak in the C_1--Br_1 pPDF. Although the first peak in the C_1--Br_1 pPDF has a much larger height than the other peaks seen in Figure 12, the area under the first peak in each of the pPDFs shown is comparable. This indicates that the C_1--Br_1 first separation distance is particularly well defined. The peak maximum occurs at approximately 3.2 Å, close to the sum of the unsolvated radius of a bromide anion (1.96 Å[35]) and the C-H bond length used for acn in the simulation (1.087 Å). This indicates that the first solvation shell is held very tightly around the bromide anions. The first peak in the N_1--Br_1 pPDF is around 4.6 Å, giving a separation between the first peaks in the C_1--Br_1 and N_1--Br_1 pPDFs of around 1.4 Å. An angle of 75 ° from the radial has been calculated for the acn molecules surrounding the bromide anions (see supplementary information section S4 for the calculation). Of the four acn-ion pPDFs shown, the C_1--Br_1 shows the largest second peak, which is around 7.4 Å. The separation between this peak and the first peak in the N_1--Br_1 pPDF is around 2.8 Å. The sum of the nitrogen van der Waals radius, the hydrogen van der Waals radius and the hydrogen-carbon bond is around 3.7 Å. This indicates that the second shell of acn molecules surrounding the bromide anion is held close to the first shell by the dipolar interactions between the acn molecules.

It should be noted that the pPDFs calculated from the simulated structures show more noise in the ion-acn and ion-ion pPDFs than the acn-acn pPDFs. This is due to the smaller number of ions in the simulation, giving a smaller sample set to base the calculations on.

Table 6 shows the coordination of each of the ions centres, N_{1c} and Br_1, by the C_1 and N_1 atoms of acn in a number of distance ranges. The electrostatic interactions between the ions and

the dipole moment of the acn mean that the TPA cation will interact more favourably with the N_1 end of the acn and the bromide anion will interact more favourably with the C_1 end. As well as being reflected in the peak positions of the pPDFs, this is also seen in the coordination of the ions by the acn, where the TPA cation shows a higher coordination number by N_1 than by C_1 at the shorter distances (2.8 and 1.0 respectively), while the bromide anion shows a higher coordination by C_1 than by N_1 (4.2 and 0.5 respectively). As the distance range goes out to higher-r the coordination numbers by the different acn atoms become more similar. This is because the larger distance ranges include the whole of the oriented molecules and possibly the beginnings of the second layer of acn molecules while the shorter ranges only include the acn ends that are closer to the ions.

The coordination for the bromide is also larger at smaller distances than that of the TPA. Again, this is expected due to the different sizes of the ions, with the TPA having a larger excluded radius than the Br anion. The coordination numbers for the cation show that if there is penetration of the solvent between the alkyl chains, it is only a very minor.

Table 6: N_{1c} and Br_1 coordination by C_1 and N_1 calculated from pPDFs.

partial	**distance of N(r) / Å**					
	3.0-5.0[a]	**3.0-5.8[b]**	**3.0-8.0[c]**	**2.0-4.0[d]**	**2.0-6.0[e]**	**2.0-8.7[f]**
N_{1c}-C_1	1.0 ± 0.8	3.8 ± 1.4	17.0 ± 1.2	--	--	--
N_{1c}-N_1	2.8 ± 1.2	5.5 ± 1.4	16.8 ± 2.5	--	--	--
Br_1-C_1	--	--	--	4.2 ± 1.4	6.8 ± 2.1	24.1 ± 4.2
Br_1-N_1	--	--	--	0.5 ± 0.7	7.9 ± 2.0	23.5 ± 3.5

a - range to slight shoulder in N_{1c}--N_1 pPDF first peak; b - range to first minima in N_{1c}--N_1 pPDF; c - range to first minima in N_{1c}--C_1 pPDF; d - range to where Br_1--C_1 pPDF first peak crosses Br_1--N_1 pPDF first peak; e - range to first minima in Br_1--N_1 pPDF; f - range to where Br_1--C_1 pPDF second peak crosses Br_1--N_1 pPDF

In order to obtain a simple picture of the solvation of the ions by acn, their coordination by the centre of the acn molecules can be considered (the C_2 atom is taken as an approximation as the centre of acn). Taking the first solvation shell of the ions to be within the first peak in the C_2-ion pPDFs (shown in Figure 13), gives solvation shell outer distances of 5.1 Å for the anion and 6.5 Å for the cation. This gives a solvation number of 5 for the anion, which is within the typical range of bromide solvation numbers found in the literature.[67,46,68] The solvation number for the cation based on the radius of 6.5 Å is 8. Comparison with the literature on tetraalkylammonium cation solvation showed that there is little consensus on what should and should not be considered to be part of the solvation shell, or what sort of numbers might be expected.[69,43,70,20]

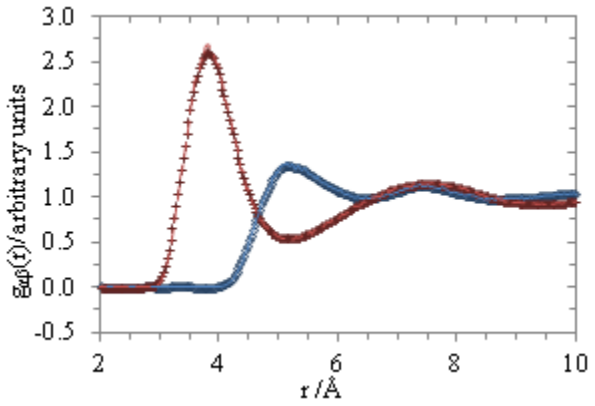

Figure 13: pPDFs calculated by EPSR from the experimental data (points) and the simulation (lines) for C_2-N_{1c} (blue diamonds and solid line) and C_2-Br_1 (red crosses and dashed line)

The ion-ion pPDFs are shown in Figure 14 There is a very sharp, intense peak in the N_{1c}--Br_1 pPDF around 3.9 Å. Not only does the sharpness of the peak indicate structured ion association, the distance is within the estimated outer radius of the TPA, indicating a degree of penetration of the anion between the alkyl chains of the cation. The intensity of this peak also indicates that there is potentially a high proportion of ion association. This N_{1c}--Br_1 peak is the only sharp peak

seen for the ion-ion interactions, as the N_{1c}--N_{1c} and Br_1--Br_1 pPDFs show only broad peaks, with very little intensity fluctuation. As such, comparing peak positions between the three ion-ion pPDFs is rather difficult. In this case, a simpler comparison can be made by considering the position of the onset of the peaks. For the N_{1c}--Br_1 pPDF this occurs around 3.3 Å, while for the N_{1c}--N_{1c} and Br_1--Br_1 pPDFs the values are 6.0 Å and 4.4 Å respectively. As expected from the relative cation and anion size, the N_{1c}--N_{1c} peak has the largest onset distance. However, at 6.0 Å, the value is smaller than the sum of two cation radii. This suggests that as well as direct ion pairing, there is also a degree of higher order ion association. In contrast the Br_1--Br_1 pPDF first peak onset distance is larger than the sum of two anion radii, suggesting there is no equivalent direct anion-anion contact to the cation-anion and cation-cation contacts. This is not unsurprising due to the smaller size of the bromide anion.

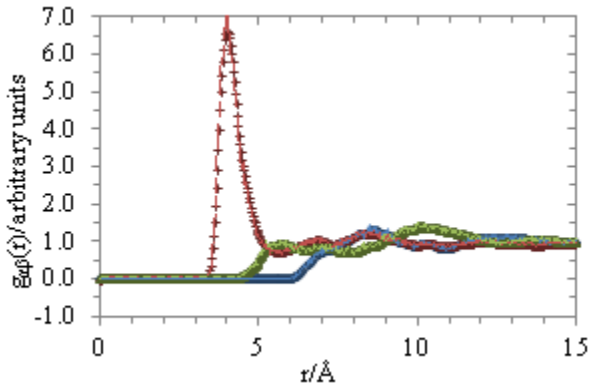

Figure 14: pPDFs calculated from the experimental data (points) and the simulation (lines) for N_{1c}--N_{1c} (blue diamonds, solid line) N_{1c}--Br_1 (red crosses, long-dashed line) and Br_1--Br_1 (green triangles, short-dashed line)

The ion pairing can be quantified by considering the arrangement of the atoms in the simulation box over a series of frames (all frames taken after the system had come to

equilibrium). Figure 15 (which shows the simulated ion arrangement for one frame) shows qualitatively that there is a high degree of ion association. By considering which ions have a Br_1--H_{1c} separation of 3 Å or less we may state what proportion of the ions are isolated, in pairs or in higher order clusters (Table 7). It turns out that nearly two thirds of the ions are associated with each other in some manner, with a little under 25 % of the ions in direct 1:1 cation:anion pairs, while a little over 40 % of the ions are in higher order clusters (e.g. 2:1 cation:anion groups). The full breakdown of the ion association is given in the supplementary information (Section S4, Tables S20 and S21).

Table 7: Percentage of ions that are isolated, in pairs or in higher order clusters

	Isolated ions	**1:1 ion pairs**	**Higher order clusters**
TPA	33.73	24.43	41.83
Br	31.18	24.43	44.38

Such association is not unexpected at this salt concentration, as the electrostatic attraction between the ions cannot be fully screened by the solvent. The Bjerrum length for acn is 1.49 nm[71], and as such for the ions to be fully screened from one another they would need to be around 15 Å apart. The ion-ion pPDFs in Figure 14 show ion-ion separations of both oppositely charged and like charged ions below this distance, so a number of the ions are likely to be interacting electrostatically with one another. In addition to this, the coordination of the ions by the acn showed that there are approximately 17 acn molecules surrounding the TPA cation within the distance range 3.0-8.0 Å from the N_{1c} atom. As there are only 19 acn molecules for each ion pair in solution, this indicates that a large proportion of the acn molecules are within the first and second solvation shells of the cation. This means there are too few acn molecules to

keep all of the ions fully separated by solvent, giving further reasons to expect ion pairing to occur.

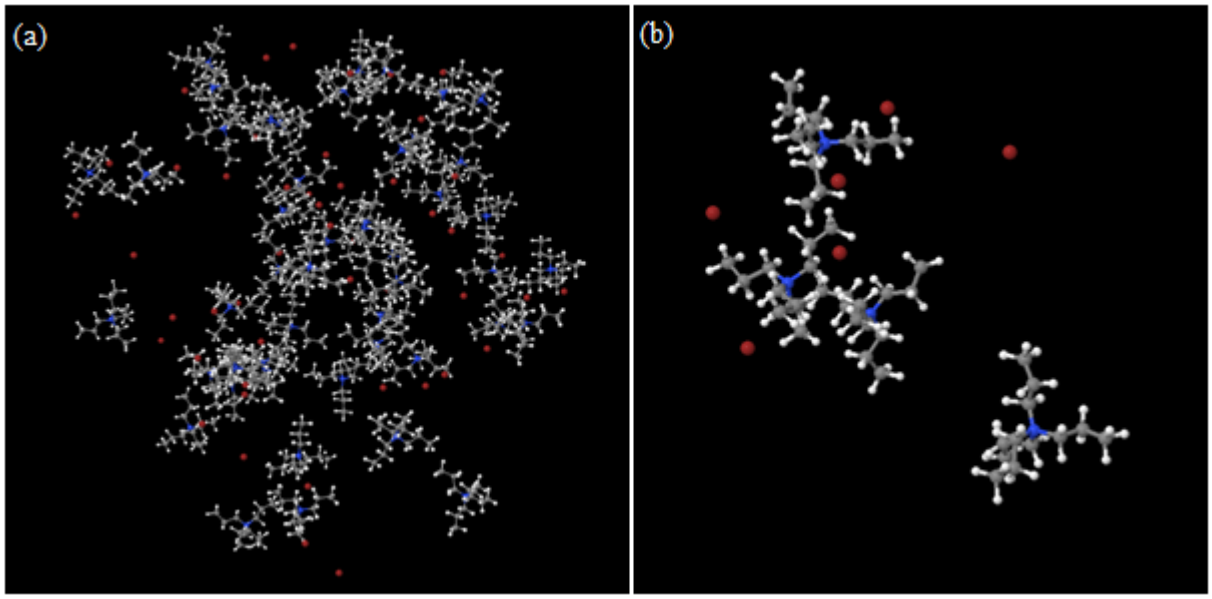

Figure 15: Images of the solution simulation box (solvent molecules not shown for clarity). Panels show a) the full box; b) a subsection (20 Å by Å 20 by 20 Å) centred around a cation.

The ion-ion coordination numbers calculated by EPSR using the pPDFs for two distance ranges are shown in Table 8. The N_{1c}--Br_1 coordination becomes non-zero within the estimated radius of the TPA cation. This indicates that, like the acn, the bromide anion may penetrate into the small gaps near the edges of the TPA cation, or at least approach the TPA outer radius. At both of the considered distance ranges the N_{1c}-Br_1 coordination is significantly larger than the N_{1c}--N_{1c} or Br_1--Br_1 coordination.

Table 8: ion-ion coordination calculated from pPDFs

partial	**distance range for N(r) / Å**	
	3.0-6.0[a]	**3.0-10.0**[b]
N_{1c}--N_{1c}	0.0 ± 0.0	1.6 ± 1.0

N_{1c}--Br_1	0.6 ± 0.7	2.2 ± 1.3
Br_1--Br_1	0.1 ± 0.3	1.5 ± 1.1

a - range to where downslope of first peak in Br_1--Br_1 pPDF crosses the N_{1c}--Br_1 pPDF; b - range to first minima in N_{1c}--N_{1c} pPDF and second minima in N_{1c}--Br_1 pPDF

As with the pure d-acn, in addition to considering the pPDFs the structure of the solution may be considered by examining the 3D spatial distribution of molecules surrounding a central molecule. In Figure 16 the distribution of all of the species around a central acn molecule is considered. The overall shape of the distribution is similar to that seen in the pure d-acn, which is unsurprising as it is affected by the shape of the central molecule. However, we can see a distinct segregation of the three different components of the solution. The cations are generally found at the nitrogen end of the acn. This fits well with the pPDF data, which showed a shorter first peak distance in the N_1--N_{1c} pPDF to the C_1--N_{1c} pPDF. The bromide anions are seen to appear mostly near the hydrogens of the acn molecule. This makes sense as it allows minimisation of the electrostatic energy based on the anion charge and the partial charges on the acn (H_1 partial charge 0.19 e). The surrounding acn molecules are mostly found around the middle section of the central acn. There are also regions of acn density at either end of the central acn. It is worth noting the different distances away from the central molecule at which the different species occur. The Br anions show spatial density closest to the central acn, the TPA cations appear at the largest distance from the central acn and the surrounding acn molecules are at an intermediate distance between that of the two ions. This is due to the different sizes of the species in solution. The Br anions are the smallest of the three species, allowing the closest approach of the centre of mass. The TPA cation, being the bulkiest species, has its centre of mass position relative to the central molecule at the largest distance. Acn molecules, intermediate in terms of size also appears at the intermediate distance.

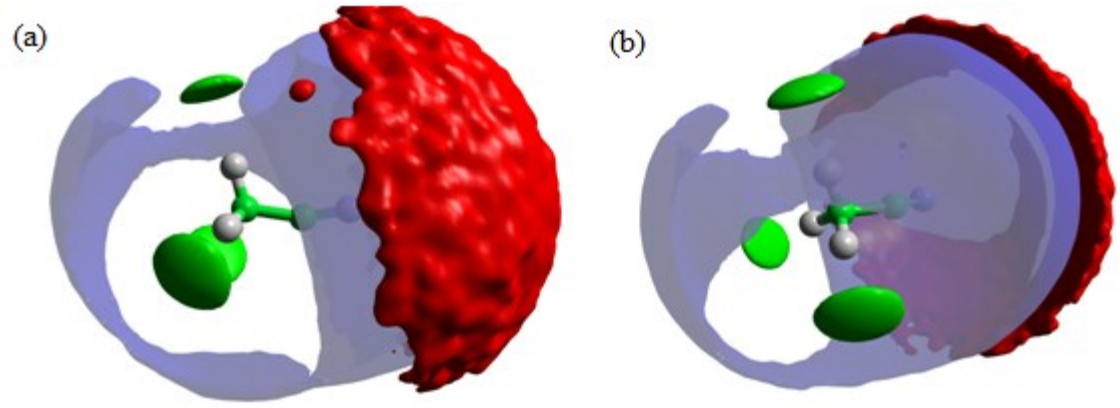

Figure 16: Spatial density distribution function of all three solution species about a central acn molecule. The acn (shown in blue), TPA (shown in red) and Br (shown in green) functions encompass surfaces representing 2.5, 2.0 and 15.0 times the bulk density of molecules in the system.

Figure 17 shows the distribution of all the species around a central cation. We can clearly see that there are no strong structural correlations between the cations, while in contrast both the acn molecules and the bromide anions show well defined spatial patterns. If the central TPA cation is considered to be approximately tetrahedral in shape, then the surrounding bromide anions show a preference to sit in the middle of the four faces of the tetrahedron. In the N_{1c}--Br_1 pPDF the first peak indicated that there is a degree of ion penetration between the alkyl arms of the cation. This corresponds nicely to the spatial density as the most accessible place to penetrate into the cation structure will be the centre of the tetrahedron's faces. The surrounding acn molecules make bridges between the areas of high anion spatial density.

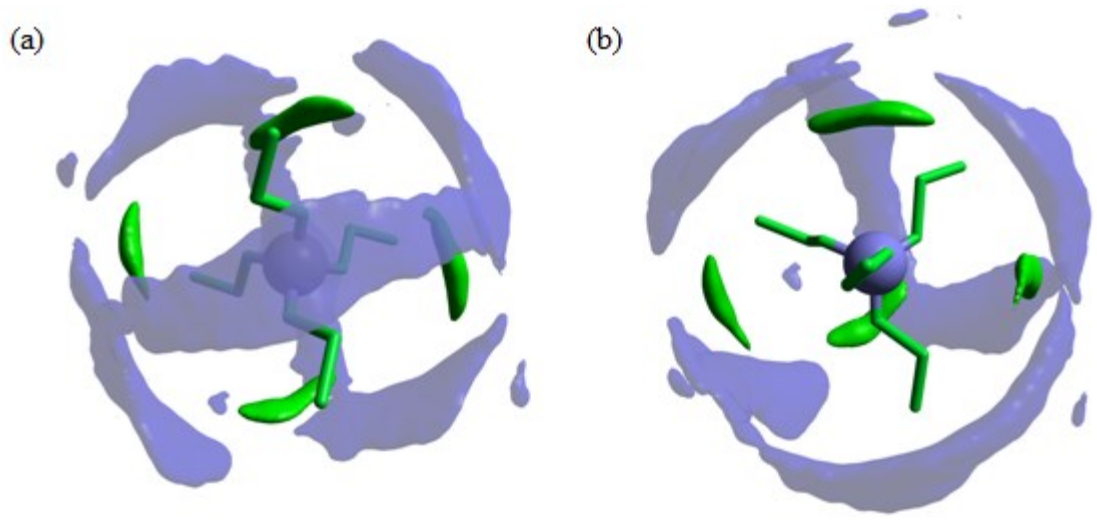

Figure 17: Spatial density distribution function of all three solution species about a central TPA molecule (hydrogen atoms not shown for clarity). The acn density is shown in blue, the TPA cation density is shown in red and the Br anion density is shown in green.

CONCLUSIONS

We have measured and analysed the bulk liquid structure of the technologically relevant electrolyte solution – 1 M tetrapropylammonium bromide in acetonitrile. We have shown that the experimental data can be modelled to a high degree of accuracy using the EPSR method, and that detailed correlations can be extracted from the simulation data. The ability to extract partial pair distribution functions allows the structural correlations of different components of the system to be separated and coordination numbers to be extracted.

We have demonstrated that there is local dipolar ordering present within liquid acn, and that the partial charges leading to this dipolar ordering also affect how the acn interacts with the ions in solution. The dipolar interactions between acn molecules are weaker than the interaction of the acn with the ions, leading to a restructuring of the acn molecules with respect to each other. The

positively charged methyl end of the acn was shown to approach more closely to the bromide anion, and the negatively charged nitrogen end to approach more closely to the tetrapropylammonium cation.

At the concentration studied we found that there is a reasonable degree of ion association (only around a third of the ions are found in isolation), and that some of the ion pairs approach together in nearly direct contact. In addition, we have extracted solvation numbers for both the TPA cation (8) and the bromide anion (5). The demonstration of ion pairing in the bulk solutions is important for their role as EDLC electrolytes, where the ions form double layers with the charged electrolyte surface. The formation of such double layers could lead to the break-up of the ion pairs, and rearrangement of the electrolyte with respect to its bulk structure. In future work the change in the electrolyte structure under confinement will be considered.

ASSOCIATED CONTENT

Supporting Information: details of template molecules (bond lengths, partial charges, etc) used in simulations; simulation setup and run details; acn simulation box size comparison; acn bond lengths and distributions; acn pPDF weighting factors and functions; experimental and simulated total structure factors for solution simulation; experimental and simulated pair correlation functions; bond lengths and distributions for acn and TPA in solution; solution pPDF weighting factors and functions; ion-acn angle calculations; ion association description.

This material is available free of charge via the Internet at http://pubs.acs.org.

AUTHOR INFORMATION

Corresponding Author

*S. M Clarke – stuart@bpi.cam.ac.uk

Author Contributions

The manuscript was written through contributions of all authors. All authors have given approval to the final version of the manuscript.

Funding Sources

E.K.H. acknowledges the European Research Council ERC Grant ERC-2009-AdG-247411 for funding.

P.K.A acknowledges a Junior Research Fellowship from Gonville and Caius College, an Oppenheimer Fellowship from the University of Cambridge.

R.J.L.W. acknowledges the EPSRC Grant 11220426 for funding.

ACKNOWLEDGMENT

We thank the staff and scientists at ISIS for the allocation of beamtime (RB1300029) and technical assistance with the scattering measurements. Thanks also to Daniel Bowron and Tom Headen for helpful discussions regarding the data analysis.

ABBREVIATIONS

EDLC, electrochemical double layer capacitor; PDF, pair distribution function; pPDF, partial pair distribution function; EPSR, empirical potential structure refinement; TPA Br, tetrapropylammonium bromide; can, acetonitrile, h-, hydrogenated; d-, deuterated.

REFERENCES

(1) Izutsu, K. *Electrochemistry in Nonaqueous Solutions*; Wiley-VCH, 2002; Vol. 5.

(2) Zoski, C. G. *Handbook of Electrochemistry*; Elsevier: London, 2007.

(3) Robinson, R. A.; Stokes, R. H. *Electrolyte Solutions*, 2nd ed.; Butterworths: London, 1970.

(4) Dufrêche, J.-F.; Bernard, O.; Turq, P.; Mukherjee, a.; Bagchi, B. Ionic Self-Diffusion in Concentrated Aqueous Electrolyte Solutions. *Phys. Rev. Lett.* **2002**, *88*, 095902.

(5) Conway, B. E. *Electrochemical Supercapacitors: Scientific Fundementals and Technological Applications*; Kluwer Academic/Plenum, 1999.

(6) Walrafen, G. E. Raman Spectral Studies of the Effects of Electrolytes on Water. *J. Chem. Phys.* **1962**, *36*, 1035–1042.

(7) Smith, J. D.; Saykally, R. J.; Geissler, P. L. The Effects of Dissolved Halide Anions on Hydrogen Bonding in Liquid Water. *J. Am. Chem. Soc.* **2007**, *129*, 13847–13856.

(8) Bergstrom, P.-A.; Lindgren, J.; Kristiansson, O. An IR Study of the Hydration of ClO4-, NO3-, I-, Br-, Cl-, and SO42- Anions in Aqueous Solution. *J. Phys. Chem.* **1991**, *95*, 8575–8580.

(9) Pieniazek, P. A.; Stangret, J. Hydration of Tetraethylammonium Tetrafluoroborate Derived from FTIR Spectroscopy. *Vib. Spectrosc.* **2005**, *39*, 81–87.

(10) Takekiyo, T.; Yoshimura, Y. Raman Spectroscopic Study on the Hydration Structures of Tetraethylammonium Cation in Water. *J. Phys. Chem. A* **2006**, *110*, 10829–10833.

(11) Loring, J. S.; Fawcett, W. R. Ion - Solvent Interactions in Acetonitrile Solutions of Lithium, Sodium, and Tetraethylammonium Perchlorate Using Attenuated Total Reflectance FTIR Spectroscopy. *J. Phys. Chem.* **1999**, *10319*, 3608–3617.

(12) Seo, J.; Cheong, B.; Cho, H. Solvation of LiClO4 and NaClO4 in Deuterated Acetonitrile Studied by Means of Infrared and Raman Spectroscopy. *Spectrochim. Acta Part A* **2002**, *58*, 1747–1756.

(13) Asada, M.; Fujimori, T.; Fujii, K.; Kanzaki, R.; Umebayashi, Y.; Ishiguro, S. Solvation Structure of Magnesium , Zinc , and Alkaline Earth Metal Ions in N,N-Dimethylformamide, N,N-Dimethylacetamide, and Their Mixtures Studied by Means of Raman Spectroscopy and DFT Calculations – Ionic Size and Electronic Effects on Steric Congestio. *J. Raman Spectrosc.* **2007**, *38*, 417–426.

(14) Seo, D. M.; Borodin, O.; Han, S.-D.; Ly, Q.; Boyle, P. D.; Henderson, W. a. Electrolyte Solvation and Ionic Association. *J. Electrochem. Soc.* **2012**, *159*, A553–A565.

(15) Allen, J. L.; Borodin, O.; Seo, D. M.; Henderson, W. A. Combined Quantum chemical/Raman Spectroscopic Analyses of Li+ Cation Solvation: Cyclic Carbonate solvents—Ethylene Carbonate and Propylene Carbonate. *J. Power Sources* **2014**, *267*, 821–830.

(16) Umebayashi, Y.; Mitsugi, T.; Fukuda, S.; Fujimori, T.; Fujii, K.; Kanzaki, R.; Takeuchi, M.; Ishiguro, S. Lithium Ion Solvation in Room-Temperature Ionic Liquids Involving Bis (trifluoromethanesulfonyl) Imide Anion Studied by Raman Spectroscopy and DFT Calculations. *J. Phys. Chem. B* **2007**, *111*, 13028–13032.

(17) Dhumal, N. R.; Noack, K.; Kiefer, J.; Kim, H. J. Molecular Structure and Interactions in the Ionic Liquid 1-Ethyl-3-Methylimidazolium Bis(Trifluoromethylsulfonyl)imide. *J. Phys. Chem. A* **2014**, *118*, 2547–2557.

(18) Harmon, K. M.; Bulgarella, J. A. Hydrogen Bonding. Part 61. Ft-NMR Study of Acetylcholine and Tetrapropylammonium Ion; Conformation and Stoichiometry of Hydration of Tetrapropylammonium Ion in Aqueous Solution. *J. Mol. Struct.* **1995**, *351*, 181–186.

(19) Luzhkov, V. B.; Osterberg, F.; Acharya, P.; Chattopadhyaya, J.; Aqvist, J. Computational and NMR Study of Quaternary Ammonium Ion Conformations in Solution. *Phys. Chem. Chem. Phys.* **2002**, *4*, 4640–4647.

(20) Bhowmik, D.; Malikova, N.; Mériguet, G.; Bernard, O.; Teixeira, J.; Turq, P. Aqueous Solutions of Tetraalkylammonium Halides: Ion Hydration, Dynamics and Ion-Ion Interactions in Light of Steric Effects. *Phys. Chem. Chem. Phys.* **2014**, *16*, 13447–13457.

(21) Cowley, J. M. *Diffraction Physics*, 2nd ed.; North-Holland Pub. Co.: Amsterdam, 1981.

(22) Egami, T.; Billinge, S. J. L. *Underneath the Bragg Peaks: Structural Analysis of Complex Materials*, 1st ed.; Pergamon, 2003.

(23) Billinge, S. J. L. The Atomic Pair Distribution Function: Past and Present. *Zeitschrift für Krist.* **2004**, *219*, 117–121.

(24) Chieux, P.; Coppens, P.; Dachs, H.; Hayter, J. B.; Lindgård, P.-A.; Petrascheck, D.; Prandl, W.; Rauch, H.; Schmatz, W.; Zaccaï, G. *Neutron Diffraction*; Dachs, H., Ed.; Springer-Verlag: New York, 1978.

(25) Botti, A.; Bruni, F.; Imberti, S.; Ricci, M. A.; Soper, A. K. Ions in Water: The Microscopic Structure of Concentrated NaOH Solutions. *J. Chem. Phys.* **2004**, *120*, 10154–10162.

(26) Botti, A.; Bruni, F.; Imberti, S.; Ricci, M. A.; Soper, A. K. Ions in Water: The Microscopic Structure of a Concentrated HCl Solution. *J. Chem. Phys.* **2004**, *121*, 7840–7848.

(27) Soper, A. K.; Weckström, K. Ion Solvation and Water Structure in Potassium Halide Aqueous Solutions. *Biophys. Chem.* **2006**, *124*, 180–191.

(28) Kameda, Y.; Miyazaki, T.; Otomo, T.; Amo, Y.; Usuki, T. Neutron Diffraction Study on the Structure of Aqueous LiNO3 Solutions. *J. Solution Chem.* **2014**, *43*, 1588–1600.

(29) Wasse, J. C.; Hayama, S.; Skipper, N. T.; Benmore, C. J.; Soper, A. K. The Structure of Saturated Lithium– and Potassium–ammonia Solutions as Studied by Using Neutron Diffraction. *J. Chem. Phys.* **2000**, *112*, 7147–7151.

(30) Deetlefs, M.; Hardacre, C.; Nieuwenhuyzen, M.; Padua, A. A. H.; Sheppard, O.; Soper, A. K. Liquid Structure of the Ionic Liquid 1,3-Dimethylimidazolium Bis {(trifluoromethyl)sulfonyl} Amide. *J. Phys. Chem. B* **2006**, *110*, 12055–12061.

(31) Bowron, D. T.; Agostino, C. D.; Gladden, L. F.; Hardacre, C.; Holbrey, J. D.; Lagunas, M. C.; McGregor, J.; Mantle, M. D.; Mullan, C. L.; Youngs, T. G. A. Structure and Dynamics of 1-Ethyl-3-Methylimidazolium Acetate via Molecular Dynamics and Neutron Diffraction. *J. Phys. Chem. B* **2010**, *114*, 7760–7768.

(32) Hayes, R.; Imberti, S.; Warr, G. G.; Atkin, R. Effect of Cation Alkyl Chain Length and Anion Type on Protic Ionic Liquid Nanostructure. *J. Phys. Chem. C* **2014**, *118*, 13998–14008.

(33) Hayes, R.; Imberti, S.; Warr, G. G.; Atkin, R. How Water Dissolves in Protic Ionic Liquids. *Angew. Chem. Int. Ed. Engl.* **2012**, *51*, 7468–7471.

(34) Hayes, R.; Bernard, S. A.; Imberti, S.; Warr, G. G.; Atkin, R. Solvation of Inorganic Nitrate Salts in Protic Ionic Liquids. *J. Phys. Chem. C* **2014**, *118*, 21215–21225.

(35) *CRC Handbook of Chemistry and Physics: a Ready-Reference Book of Chemical and Physical Data*, 90th ed.; Lide, D. R., Haynes, W. M., Eds.; CRC Press: London, 2009.

(36) Bertagnollia, H.; Zeidlera, M. D. Molecular Pair-Correlation Function of Liquid Acetonitrile from X-Ray and Neutron-Diffraction Studies. *Mol. Phys.* **1978**, *35*, 177–192.

(37) Fries, P. H.; Richardi, J.; Krienke, H. Dielectric and Structural Results for Liquid Acetonitrile, Acetone and Chloroform from the Hypernetted Chain Molecular Integral Equation. *Mol. Phys.* **1997**, *90*, 841–854.

(38) Takamuku, T.; Tabata, M.; Yamaguchi, A.; Nishimoto, J.; Kumamoto, M.; Wakita, H.; Yamaguchi, T. Liquid Structure of Acetonitrile-Water Mixtures by x-Ray Diffraction and Infrared Spectroscopy. *J. Phys. Chem. B* **1998**, *102*, 8880–8888.

(39) Grabuleda, X.; Jaime, C.; Kollman, P. A. Molecular Dynamics Simulation Studies of Liquid Acetonitrile: New Six-Site Model. *J. Comput. Chem.* **2000**, *21*, 901–908.

(40) Oldiges, C.; Wittler, K.; Tonsing, T.; Alijah, A. MD Calculated Structural Properties of Clusters in Liquid Acetonitrile/water Mixtures with Various Contents of Acetonitrile. *J. Phys. Chem. A* **2002**, *106*, 7147–7154.

(41) Böhm, H. J.; McDonald, I. R.; Madden, P. A. An Effective Pair Potential for Liquid Acetonitrile. *Mol. Phys.* **2006**, *49*, 347–360.

(42) Slusher, J. T.; Cummings, P. T. Molecular Simulation Study of Tetraalkylammonium Halides. 1. Solvation Structure and Hydrogen Bonding in Aqueous Solutions. *J. Phys. Chem. B* **1997**, *101*, 3818–3826.

(43) Marcus, Y. Tetraalkylammonium Ions in Aqueous and Non-Aqueous Solutions. *J. Solution Chem.* **2008**, *37*, 1071–1098.

(44) Heyda, J.; Lund, M.; Oncak, M.; Slavicek, P.; Jungwirth, P. Reversal of Hofmeister Ordering for Pairing of NH4+ Vs Alkylated Ammonium Cations with Halide Anions in Water. *J. Phys. Chem. B* **2010**, *114*, 10843–10852.

(45) Polydorou, N. G.; Wicks, J. D.; Turner, J. Z. Hydrophobic Interaction of Tetrapropylammonium Ions in Water: A Neutron Diffraction and Reverse Monte Carlo Study. *J. Chem. Phys.* **1997**, *107*, 197.

(46) Tanida, H.; Sakane, H.; Watanabe, I. Solvation Structures for Bromide Ion in Various Solvents by Extended X-Ray Absorption Fine Structure. *J. Chem. Soc. Dalt. Trans.* **1994**, 2321–2326.

(47) Ayala, R.; Martínez, J. M.; Pappalardo, R. R.; Marcos, E. S. Theoretical Study of the Microsolvation of the Bromide Anion in Water, Methanol, and Acetonitrile: Ion−Solvent Vs Solvent−Solvent Interactions. *J. Phys. Chem. A* **2000**, *104*, 2799–2807.

(48) Böes, E. S.; Livotto, P. R.; Stassen, H. Solvation of Monovalent Anions in Acetonitrile and N,N-Dimethylformamide: Parameterization of the IEF-PCM Model. *Chem. Phys.* **2006**, *331*, 142–158.

(49) Fischer, H. E.; Barnes, A. C.; Salmon, P. S. Neutron and x-Ray Diffraction Studies of Liquids and Glasses. *Reports Prog. Phys.* **2006**, *69*, 233–299.

(50) Bowron, D. T.; Finney, J. L.; Soper, A. K. Structural Investigation of Solute-Solute Interactions in Aqueous Solutions of Tertiary Butanol. *J. Phys. Chem. B* **1998**, *102*, 3551–3563.

(51) Keen, D. A. A Comparison of Various Commonly Used Correlation Functions for Describing Total Scattering. *J. Appl. Crystallogr.* **2001**, *34*, 172–177.

(52) Soper, A. K. Empirical Potential Monte Carlo Simulation of Fluid Structure. *Chem. Phys.* **1996**, *202*, 295–306.

(53) Soper, A. K. Tests of the Empirical Potential Structure Refinement Method and a New Method of Application to Neutron Diffraction Data on Water. *Mol. Phys.* **2001**, *99*, 1503–1516.

(54) Soper, A. K. Partial Structure Factors from Disordered Materials Diffraction Data: An Approach Using Empirical Potential Structure Refinement. *Phys. Rev. B* **2005**, *72*, 104204.

(55) Bowron, D. T.; Soper, a K.; Jones, K.; Ansell, S.; Birch, S.; Norris, J.; Perrott, L.; Riedel, D.; Rhodes, N. J.; Wakefield, S. R.; et al. NIMROD: The Near and InterMediate Range Order Diffractometer of the ISIS Second Target Station. *Rev. Sci. Instrum.* **2010**, *81*, 033905.

(56) Soper, A. K.; Howells, W. S.; Hannon, A. C. *ATLAS - Analysis of Time-of-Flight Diffraction Data from Liquid and Amorphous Materials*; 1989; pp RAL–89–046.

(57) Soper, A. K. The Radial Distribution Function of Water as Derive from Radiation Total Scattering Experiments: Is There Anything We Can Say for Sure? *ISRN Phys. Chem.* **2013**, *2013*, 279463.

(58) Acetonitrile-d3 MSDS http://www.chemicalbook.com/ChemicalProductProperty_EN_CB6289320.htm (accessed Jul 26, 2014).

(59) Stewart, J. MOPAC http://openmopac.net/ (accessed Oct 29, 2014).

(60) Pauling, L.; Springall, H.; Palmer, K. The Electron Diffraction Investigation of Methylacetylene, Dimethylacetylene, Dimethyldiacetylene, Methyl Cyanide, Diacetylene, and Cyanogen. *J. Am. Chem. Soc.* **1939**, *123*, 927–937.

(61) Danford, M.; Livingston, R. The Molecular Structure of Methyl Cyanide and Trifluoromethyl Cyanide by Electron Diffraction1. *J. Am. Chem. Soc.* **1955**, *77*, 2944–2947.

(62) Costain, C. C. Determination of Molecular Structures from Ground State Rotational Constants. *J. Chem. Phys.* **1958**, *29*, 864.

(63) Kratochwill, V. A.; Weidner, J. U.; Zimmermann, H. Rontgenstrukturuntersuchung Des Flussigen Acetonitrils. *Berichte der Bensengesellschaft fur Phys. Chemie* **1973**, *77*, 408.

(64) Bertagnolli, H.; Chieux, P.; Zeidler, M. D. A Neutron-Diffraction Study of Liquid Acetonitrile. *Mol. Phys.* **1976**, *32*, 759–773.

(65) Nikitin, A. M.; Lyubartsev, A. P. New Six-Site Acetonitrile Model for Simulations of Liquid Acetonitrile and Its Aqueous Mixtures. *J. Comput. Chem.* **2007**, *48*, 2020–2026.

(66) Riley, K. F.; Hobson, M. P.; Bence, S. J. *Mathematical Methods for Physics and Engineering*, 3rd ed.; Cambridge University Press: Cambridge, 2006.

(67) Hinton, J. F.; Amis, E. S. Solvation Numbers of Ions. *Chem. Rev.* **1971**, *71*, 627–674.

(68) Ayala, R.; Martinez, J. M.; Pappalardo, R. R.; Muñoz-Paez, A.; Sanchez Marcos, E. The Solvation of Bromide Anion in Acetonitrile: A Structural Study Based on the Combination of Theoretical Calculations and X-Ray Absorption Spectroscopy. *Mol. Simul.* **2007**, *32*, 1035–1043.

(69) Symons, M. C. R. On the Possible Solvation of Tetraalkyl-Ammonium Cations and Tetraphenyl-Boron Anions by Water. *Phys. Chem. Chem. Phys.* **1999**, *1*, 113–114.

(70) Hemalatha, B.; Vasantharani, P.; Vijayakumari, K. K. Ion-Ion and Ion-Solvent Interactions of Tetraalkyl Ammonium Bromide in Mixed DMF-Water Systems at Different Temperatures. *J. Solution Chem.* **2009**, *38*, 947–955.

(71) Giesecke, M.; Mériguet, G.; Hallberg, F. Ion Association in Aqueous and Non-Aqueous Solutions Probed by Diffusion and Electrophoretic NMR. *Phys. Chem. Chem. Phys.* **2015**, *17*, 3402–3408.

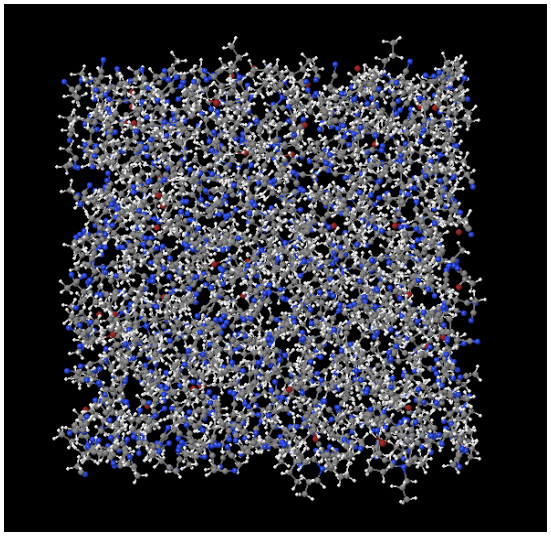

Figure 18: Table of contents graphic